Journal of Molecular Modeling (2018) 24: 200
https://doi.org/10.1007/s00894-018-3742-4

ORIGINAL PAPER

Electrical tree inhibition by SiO_2/XLPE nanocomposites: insights from first-principles calculations

Xiaonan Zheng[1] · Yang Liu[1] · Ya Wang[1]

Received: 5 April 2018 / Accepted: 27 June 2018 / Published online: 9 July 2018

Abstract

It has been extensively observed in experiments that nanoparticle additives can efficiently inhibit the electrical tree growth of the cross-linked polyethylene (XLPE) matrix of power cables. Inspired by this, the first-principles calculations employing the density functional theory (DFT) method were performed in this study to investigate the significant role of SiO_2 nanosized fillers as a voltage stabilizer for power cable insulation. Several different types of α-SiO_2 fillers, including hydroxylated, reconstructed, doped or oxygen vacancy surface structures, were constructed to model the interfacial interaction for SiO_2/XLPE nanocomposites. It is found that the SiO_2 additives can restrict the movement of the polyethylene chain through van der Waals physical interaction. More importantly, based on the Bader charge analysis we reveal that SiO_2 could effectively capture hot electrons to suppress space charge accumulation in XLPE. However, some particular modified-surface SiO_2, such as incompletely hydroxylated, B-doped, and oxygen vacancy defect on the top layer, could induce the H migration reaction and consequent electrical tree growth of the XLPE chain. In contrast, the SiO_2 particles that have N-doped or oxygen vacancy on the lower layer with completely hydroxylated surfaces, as well as the reconstructed surface, are predicted to be favorable additives because of their quite strong physical interaction and very weak chemical activity with XLPE. The present study is useful to understand the mechanism of the nanosized voltage stabilizer and also provide important information for further experimental investigation.

Keywords Electrical tree inhibition · SiO_2 · Cross-linked polyethylene · Density functional theory · Interfacial interaction

Introduction

Cross-linked polyethylene (XLPE) has been widely used in power cable insulation due to its excellent corrosion resistance, electrical properties, and chemical stability [1–3]. However, after a long period of operation under the high-voltage direct current (DC) field, it will accelerate ageing and damage because of the space charge accumulation and the electrical tree growth that cause irreversible changes in material properties and reduce insulation performance [4–7]. Many factors can induce the electrical treeing and the degradation of power cable insulation, such as the attack of hot electrons, local magnetic field effect produced by high current, the influence from water or temperature, and so on [8–10]. So suppressing the space charge accumulation and preventing the electrical tree growth are the key strategies to improve the lifetime of the power cable insulation. The previous studies focused on revealing the aging mechanism and developing methods to improve the electrical tree resistance [11–15]. Ieda et al. found that the breakdown property of polymer solids was governed by many complicated factors, such as volume effect, time effect, and defects [16]. To clarify the mechanism of electrical tree growth, Vaughan et al. studied the structures and chemical reaction processes of two electrical trees using confocal Raman microprobe spectroscopy, optical microscopy, and scanning electron microscopy [17]. Chen et al. investigated the electrical tree growth in XLPE cable insulation through an embedded needle electrode and found some branches which have conducting walls due to a

Electronic supplementary material The online version of this article (https://doi.org/10.1007/s00894-018-3742-4) contains supplementary material, which is available to authorized users.

✉ Yang Liu
yang.liu@hit.edu.cn

[1] MIIT Key Laboratory of Critical Materials Technology for New Energy Conversion and Storage, School of Chemistry and Chemical Engineering, Harbin Institute of Technology, Harbin 150080, People's Republic of China

layer of graphitic carbon, providing a means of early detection of prebreakdown phenomena in cable insulation [18].

In recent years, experimental studies indicated that nanosized particles are very promising fillers in power cable insulation to suppress the growth of electrical tree and prevent the degradation of polymer matrix [19–21]. Tanaka et al. conducted a comprehensive experimental investigation for XLPE and fumed silica (SiO_2), and found that SiO_2 nanocomposites additives could be applied extensively in the fields of extruded HV and EHV cables [22]. Zhang et al. used titanate coupling agent (TC9) and 3-(Methacryloyloxy)propyltrimethoxysilane (KH570) to modify the SiO_2 surface, which greatly improved the DC conductivity, dielectric characteristics, and space charge properties in XLPE/SiO_2 nanocomposites [23]. Li et al. proved that the addition of nano-Al_2O_3 fillers is also a good approach to raise once-lowered breakdown strength and the partial discharge resistance to protect the power cable [24]. Similarly, Ding and Varlow investigated treeing phenomena in epoxy-ZnO nanocomposites and found that the addition of a small amount (0.5 to 1 wt%) of zinc oxide particles in the epoxy insulation could extend the treeing time to breakdown [25]. Wang et al. explored the interface characteristics between SiC and XLPE using the pulsed-electro-acoustic (PEA) equipment and a dielectric analyzer and found that the best activity of electrical tree inhibition is achieved when the concentration of nanocomposite is 1 wt% [26]. Recently, Xiao et al. revealed the significant influence of TiO_2 nanoparticles on the dielectric properties of TiO_2/XLPE nanocomposites to suppress the space charge by PEA measurements [27]. Besides experimental studies, there are also many theoretical researches concentrating on this topic. By performing the quantum mechanics/molecular dynamics (QM/MD) simulations, Han et al. observed double electric layers around the SiO_2 nanocluster and revealed the function of the SiO_2 nanocluster as a stabilizer in trapping electrons [28]. More recently, a series of potential graphene-based particles candidates (N-doped single-vacancy graphene, graphene oxide, and B, N, Si, or P-doped graphene oxide) were predicted by the density functional theory method to be effective additives in power cables [29].

Although many experimental studies have proposed the promising SiO_2 nanocomposites fillers, further theoretical study is desired to clarify the electronic interaction between the SiO_2 fillers and the polymer matrix, as well as to design more efficient SiO_2 particles with improved surface or bulk structures. The α-quartz (α-SiO_2) is one of the most abundant and economical minerals with a wide range of applications, including high-frequency devices [30, 31], cellular and satellite network [32, 33], and quartz crystal microbalance [34–36]. Lots of experimental investigations showed that the α-SiO_2 (001) surface is the most stable one [37–40], and the 1×1 pattern [41] and $\sqrt{84} \times \sqrt{84}$ reconstruction [42] are two kinds of popular crystallographic structures. Additionally, many models with the modified surfaces were constructed for increasing reaction rate and improving the adsorption effect, such as the dense model with a six-member ring and a triangle-like structure [39, 43], the hydroxylated model yielding silanol groups [44], the one with special point defects [45, 46], and the N or B-doped models [47–50]. Consequently, such abundant surface properties of α-SiO_2 will greatly affect the interfacial interaction with XLPE, as well as the performance of XLPE/SiO_2 nanocomposites in power cable insulation. With this expectation, we employed the first-principles calculations to investigate the electrical tree inhibiting mechanism of the SiO_2 nanosized fillers with several different modified-surface structures by evaluating their ability of trapping hot electrons and restraining space charge. It is expected to provide valuable guidelines to develop potential candidates as additives in power cable insulation.

Computational methods and models

Computational methods

The density functional theory (DFT) calculations were performed using the Vienna Ab-Initio Simulation Package (VASP) [51–53] with Perdew-Burke-Ernzerhof (PBE) functional [54]. The DFT-D2 method was employed to evaluate the van der Waals interaction in the geometry optimizations. The projected-augmented wave (PAW) method [55] was used to treat the interaction between valence electrons and ion cores. A $2 \times 2 \times 1$ Monkhorst–Pack k-point mesh and a cut-off energy of 850 eV were selected for all calculations until the energy and forces of atoms were smaller than 1.0×10^{-5} eV and 0.01 eV/Å, respectively. These parameters were tested to make sure that the differences of absolute energies were well converged (within a few meV). The charge distribution was obtained by using a real-space Bader-charge analysis [56–58] based on so-called zero flux surfaces to divide atoms on which the charge density is a minimum perpendicular to the surface. The energy profiles along the reaction pathways were computed with the climbing image nudged elastic band (CI-NEB) method, then the transition state and reaction energy barrier were also determined [59, 60].

Theoretical models

Based on the α-SiO_2 (001) surface, six types of models were constructed as listed in Fig. 1. The completely hydroxylated SiO_2 (denoted as H-SiO_2) has herringbone structure and a zigzag hydrogen bonded network with short and long hydrogen bonds. Each oxygen dangling bond at the bottom atomic layer was saturated with one hydrogen atom. The dense surface, i.e., reconstructed surface (denoted as R-SiO_2), was built according to Rignanese's prediction [39]. As we know, doping

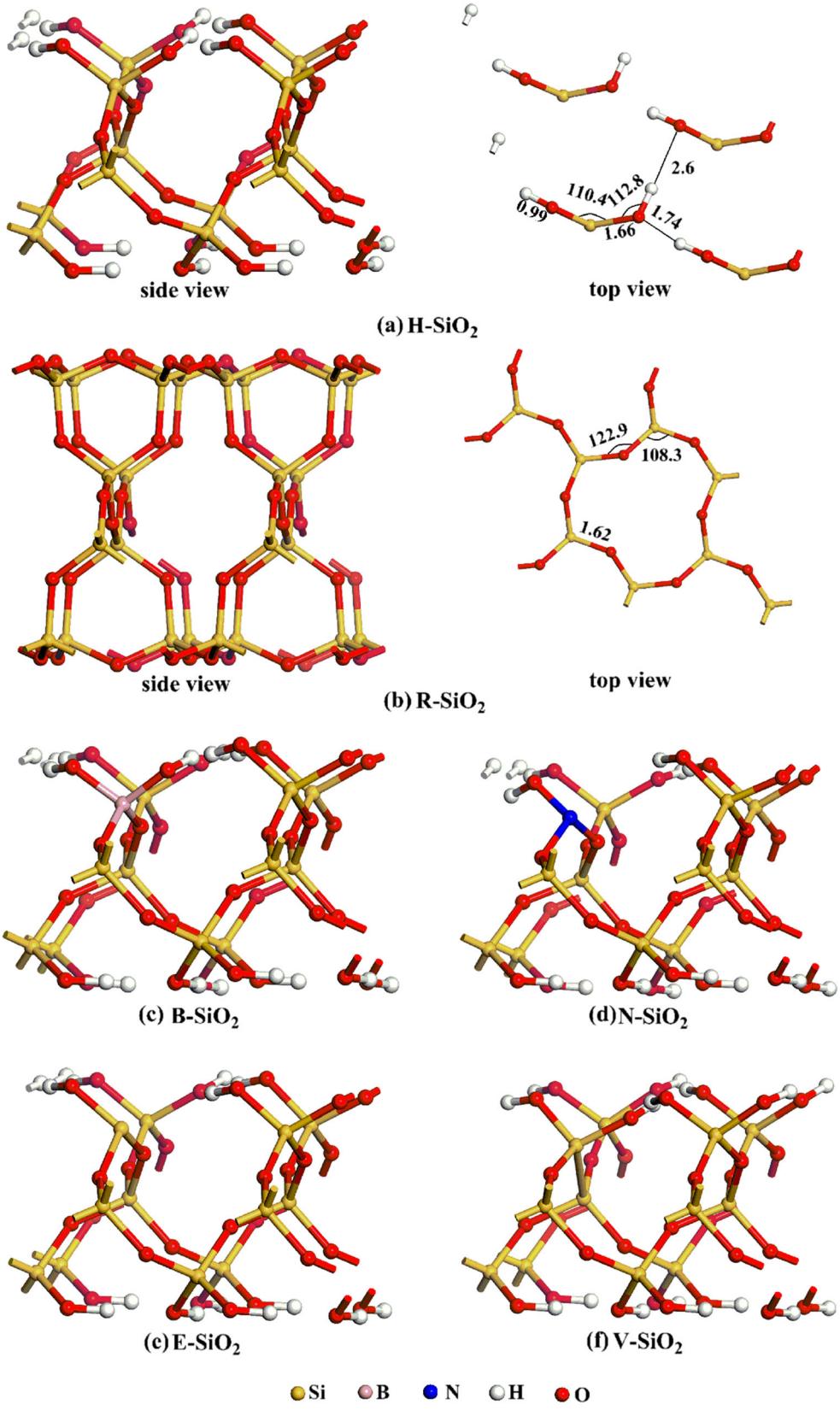

Fig. 1 **a**~**f** The SiO_2 models with optimized surface structures (side view). Top views of H-SiO_2 and R-SiO_2 are also given with labeling of the key bond lengths in Å and angles in degree (For clarity, only surface atoms are shown)

B or N could improve the material's toughness, oxidation resistance, thermal stability, etc. by introducing active sites [48, 61]. So B-doped and N-doped SiO_2 models were constructed and denoted as B-SiO_2 and N-doped SiO_2,

respectively. Two types of oxygen vacancy defect models were built by removing one oxygen atom on the top layer and the one connecting two SiO_2 tetrahedrons on the lower layer, which are denoted as E-SiO_2 and V-SiO_2, respectively. The 2 × 2 supercell with nine atomic layers was constructed to model the bulk region of the cell. For improving the computational efficiency, four atomic layers on the bottom were fixed during the optimization. A vacuum layer of 15 Å was set to minimize the periodic interaction. The 2-methylbutane C_5H_{12} [i.e., $CH_3CH(CH_3)CH_2CH_3$], including one tertiary carbon to represent cross-linked point, was used to model XLPE and simulate its activity on the surface of the SiO_2 nanoparticle. With this theoretical model, the local interfacial interaction between XLPE and SiO_2 particles and the catalytic activity of SiO_2 for XLPE were considered properly. To avoid any weak van der Waals interaction between the adsorbed molecules, we ensured that the nearest distance of two C_5H_{12} molecules in the neighborhood lattice was more than 5.0 Å.

Results and discussion

To reveal the mechanism of improving the anti-ageing properties and performance of XLPE by adding SiO_2 particles, the electrical properties of a series of SiO_2/XLPE nanocomposites were analyzed concerning the surface structures, interfacial interaction, H migration reaction activity, and space charge behavior.

Surface structures

Figure 1 shows the optimized SiO_2 models with key bond lengths and bond angles. For H-SiO_2, one can see that all O–Si–O angles (~110°) are symmetry equivalent and all the silicon atoms are fully four-coordinated. The optimized lattice parameters (a = b = 5.05 Å and c = 5.50 Å) are well matched with experimental values (a = b = 4.92 Å and c = 5.41 Å) [62], and the calculated bond lengths of H–O and O–Si are also consistent with the values optimized with PW91 and B3LYP functional [37]. For R-SiO_2, there are only four-coordinated Si and two-coordinated O atoms without any dangling bond. The predicted Si–O bond lengths (1.62 Å) and the Si–O–Si angles (122.9°) match well with previous results by Rignanese et al. [39] and Oleksandr et al. [63] using respective local density approximation (LDA) and PBE method. In B-SiO_2 where one Si atom is substituted by B atom, the B atom still connects with four O atoms, keeping the BO_4 center. In comparison, when one Si atom is replaced by N atom to form N-SiO_2, only the NO_3 skeleton is stabilized due to the rupture of one N–O bond. After removing one oxygen atom at the top layer of SiO_2, there will be a three-coordinated Si atom to form E-SiO_2. The bond length of Si–O bond (1.65 Å) is quite similar to that in H–SiO_2 (1.66 Å), indicating that oxygen vacancy defect in E-SiO_2 does not significantly change the geometrical structure. As the other point defect model, i.e., V–SiO_2, the oxygen atom connecting two SiO_2 tetrahedrons is absent and then an extra Si–Si bond is formed. The optimized Si–Si bond length with the value of 2.50 Å coincides with those obtained by employing the MP2 method [64] and B3LYP functional [65]. It is worth noting that for the models mentioned above, the obtained lattice parameters and key geometrical parameters are in good agreement with those in the literature with larger unit cell size, confirming that the present models are reliable. The electric dipole moments of different SiO_2 cells were calculated and listed in Table 1. It is found that these values are very small, indicating that the doping or defect does not affect the property of polarization too much. Based on the discussion above, it is obvious to conclude that the doping, reconstruction, or defect can cause the surface structural change of SiO_2 to different extents, and what is more, they will affect the electronic properties of surfaces by introducing many active sites and further influence the interfacial interaction with the XLPE chain.

Interfacial interaction

It is well known that the XLPE chain has a tendency of free movement, which probably accelerates the electrical tree generation with the attack of hot electrons. The SiO_2 additives are capable of generating physical interaction with XLPE to constrain the movement of polyethylene chains. In this regard, accurate adsorption energy calculations will be of crucial importance to evaluate the intensity of physical interaction.

For each system, the adsorption energy (E_{ads}) is calculated as follows:

$$E_{ads} = E(C_5H_{12} + SiO_2) - E(C_5H_{12}) - E(SiO_2)$$

where $E(C_5H_{12} + SiO_2)$ is the total energy of the SiO_2 surface with the adsorbed C_5H_{12}, $E(C_5H_{12})$ and $E(SiO_2)$ are the energies of the C_5H_{12} molecule and SiO_2 surface, respectively.

Table 1 The dipole moment (D) of SiO_2 surfaces, adsorption distances, adsorption energies (E_{ads}) between C_5H_{12} and SiO_2, and the summarized Bader charge values at SiO_2 surface

Models		D/Debye	Distance/Å	E_{ads}/eV	Charge
H-SiO_2	hydroxylated	−0.01	1.55	−0.29	0.02
R-SiO_2	reconstructed	−0.03	2.16	−0.28	0.03
B-SiO_2	B-doped	−0.03	1.53	−0.32	−0.14
N-SiO_2	N-doped	0.17	1.59	−0.41	−0.56
E-SiO_2	oxygen vacancy	0.03	2.98	−0.10	0.05
V-SiO_2	oxygen vacancy	−0.06	1.90	−0.23	0.04

The adsorption distances and adsorption energies between C_5H_{12} and SiO_2 surfaces in the optimized structures are collected in Table 1. As shown in Table 1, one can see that the C_5H_{12} molecule usually locates 1.5~3.0 Å away from different SiO_2 surfaces, and the adsorption energies vary from −0.10 to −0.41 eV, showing the pattern of van der Waals interaction between them and the characteristic of general physical adsorption. Among all the models, the N-SiO_2 is the most active surface with the lowest E_{ads} of −0.41 eV, while E-SiO_2 is the most inactive one with the highest E_{ads} of −0.10 eV. By contrast, the other H-SiO_2, R-SiO_2, B-SiO_2, and V-SiO_2 surfaces have moderate and almost similar adsorption ability for C_5H_{12} with E_{ads} of around −0.30 eV. In general, a larger adsorption intensity indicates a stronger capacity to constrain the movement of the polyethylene chain. Thus, the N-doped SiO_2 is predicted to show the best performance among all the SiO_2 additives mentioned above, and it is expected to be a potential candidate as effective additives in power cable insulation. Remarkably, the N-SiO_2 plays a significant role in transferring charges from XLPE compared with others. By analyzing the Bader charge distribution of atoms belonging to SiO_2 and C_5H_{12}, we obtained the transferred charge values as collected in Table 1. It shows that the summarized Bader charge value at the N-SiO_2 surface is −0.56, which displays the strongest ability to attract the charge from the adsorbed C_5H_{12} molecule among all SiO_2 surfaces and then effectively inhibits the space charge accumulation of the XLPE. More details of space charge behavior, will be discussed in the "Space charge behavior" section.

As a summary, we come to a short conclusion that the SiO_2 additives could restrict the movement of the polythene chain at different levels through van der Waals physical adsorption, and the N-doping is desired as a good strategy to modify the surface structure of SiO_2 in order to strengthen the interfacial interaction.

H migration reaction activity

All the models mentioned above have completely hydroxylated surface structure except R-SiO_2. However, in the real experimental operations, the SiO_2 nanoparticles with incompletely hydroxylated surfaces are very common. So we constructed an incompletely hydroxylated SiO_2 model by removing one H atom on the top layer of H-SiO_2 surface, and investigated its adsorption activity for C_5H_{12}. It was found that the H atom of C_5H_{12} could migrate easily to the unsaturated O atom, leading to the breaking of the C–H bond and the formation of a new H–O bond. The calculated adsorption energy (−1.80 eV) is much lower than those of other models studied above. The typical chemical adsorption activity will destroy the structure of XLPE and finally induce the electrical tree growth. Therefore, the SiO_2 nanoparticles with incompletely hydroxylated surfaces are not beneficial for protecting XLPE. This provides important information for the experimental treatment of the SiO_2 additives. On the other hand, it inspires us to investigate the H migration reaction activity of other SiO_2 additives, even though they could stabilize the C_5H_{12} with a certain adsorption distance.

We then employed the CI-NEB method to determine the H migration reaction pathways from C_5H_{12} to the surfaces mentioned above. For H-SiO_2, N-SiO_2, V-SiO_2, and R-SiO_2, we found that no stable H migration products could be obtained, suggesting that H migration reactions cannot happen between these surfaces and the C_5H_{12} molecule. Despite that we intended to elongate the C–H distance of C_5H_{12} and set the H atom approaching to the surface as the initial structure, the geometrical optimization for the system still converged to the previous stable C_5H_{12} adsorbed structure, i.e., the H atom went back to the C_5H_{12} part again. The possible reason is that there is no dangling bond or active sites on these surfaces which can accept an extra hydrogen atom. In the cases of B-SiO_2 and E-SiO_2 systems, however, the situations are quite different. The reaction pathways for H migration from C_5H_{12} to the B-SiO_2 or E-SiO_2 have been successfully determined and illustrated in Figs. 2 and 3, respectively. As shown in Fig. 2, the H atom in C_5H_{12} migrates gradually to the hydroxyl connecting with B atom in B-SiO_2 to yield one H_2O molecule, and meanwhile the B–O bond is broken. It is a barrierless and exothermic reaction process with reaction energy of −1.02 eV, showing a very favorable process in energy. It is interesting to know why H migration can happen easily on this surface, but not on others. We believe that the B-doping effect may play a key role in it. The B-doping could keep the main skeleton of SiO_2 where the B atom is four-coordinated. However, the B–O bonds are elongated (~1.48 Å) in comparison with those in the three-coordinated B atom (~1.34 Å), as denoted in Fig. 2, which shows that the formers are weakened. By accepting the transferred H atom, this B–O bond is broken and a water molecule is formed, resulting in a more stable planar BO_3 center. With respect to the H migration reaction on oxygen vacancy E-SiO_2 surface, as shown in Fig. 3, when the C–H bond is elongated to be 1.50 Å, the transition state (TS) is reached, in which the distance between H and Si is shortened to be 1.66 Å. In the product, the distance between H and Si is 1.47 Å, indicating that a new H–Si bond is formed. This process needs to overcome an activation barrier of 0.46 eV with the reaction energy of 0.04 eV, indicating that it may happen at room temperature. Thus, it can be concluded that B-SiO_2 and E-SiO_2 are not appropriate additives in power cable insulation due to the potential damage to XLPE.

Chemical activity is also a key factor to evaluate the performance of additives in power cable insulation. If the H atom of XLPE could migrate easily to the SiO_2 surface to form a more stable structure, it will lead to the formation of a carbon center radical. This radical could either cross-link with other radicals to affect the stability of the XLPE chain, or react with

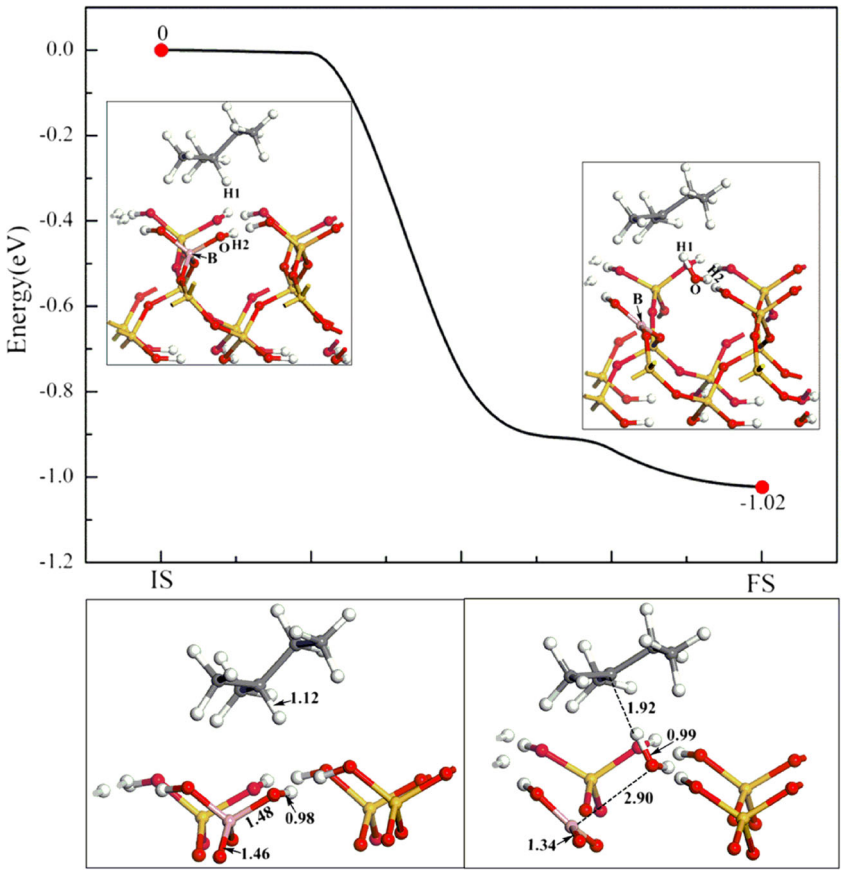

Fig. 2 The H migration reaction pathway on B-SiO_2 surface. The key bond distances in Å are denoted at the bottom by showing related atoms at top layers

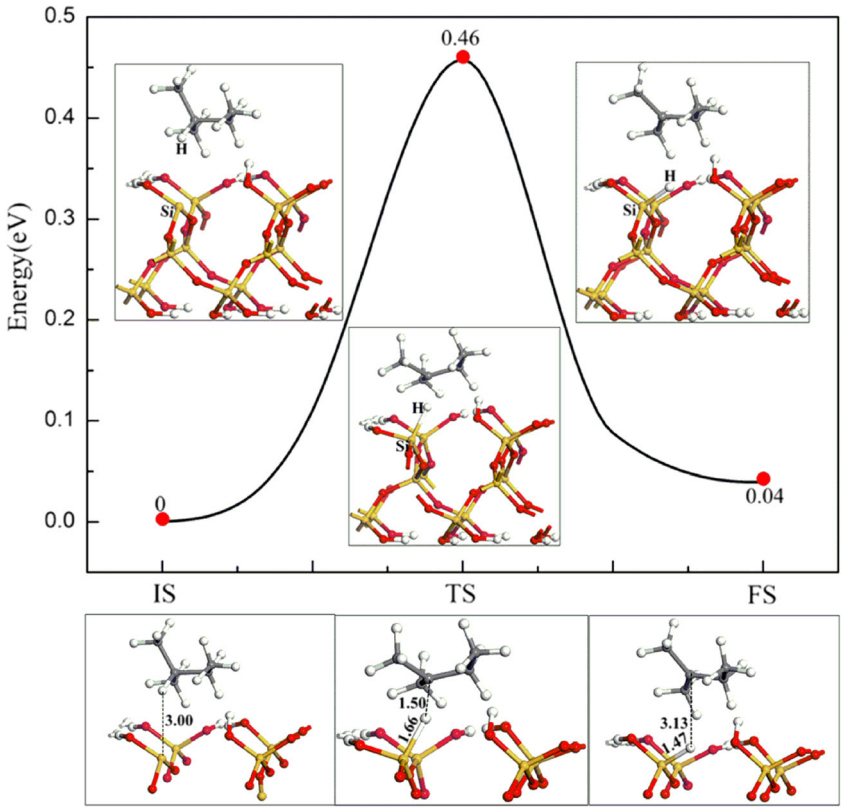

Fig. 3 The H migration reaction pathway on E-SiO_2 surface. The key bond distances in Å are denoted at the bottom by showing related atoms at top layers

other impurity substances to induce the growth of electrical treeing. According to the analysis of H migration reaction activity above, we screen out the H-SiO_2, N-SiO_2, and V-SiO_2 with completely hydroxylated surfaces, as well as the reconstructed R-SiO_2 as effective additives in power cable insulation.

Space charge behavior

When the cable insulation ages because of corrosion, high temperature, and dampness, there will be space charges accumulation. The space charge with high energy is usually called "hot electron". It was generally observed that the increase of space charge accumulation in XLPE produces a deteriorative effect on the long-term operation and reliability of insulation materials. In this section, the ability of capturing hot electrons of SiO_2 was investigated based on the Bader charge analysis. One or two extra electrons are injected respectively into the system to model the existence of hot electrons, denoted as ionic states. The charge distributions were obtained through summarizing the charge values of atoms belonging to C_5H_{12} or SiO_2 substrates, respectively.

Figure 4 depicted Bader charge results of neutral state and ionic states. For neutral state, only B-SiO_2 and N-SiO_2 surfaces have a relatively strong ability to attract electrons from C_5H_{12}, resulting in the distribution of negative charges on their surfaces (−0.14 for B-SiO_2, and −0.56 for N-SiO_2), as listed in Table 1. When one electron is injected to the system, one can see that the electron density mainly locates on the SiO_2 additive, but not at C_5H_{12}. In particular, the charge values of B-SiO_2, E-SiO_2, and N-SiO_2 are up to −0.92, −0.92, and − 1.17, respectively. When injecting two electrons, SiO_2 still carries negative charges in large quantity. Especially for N-SiO_2, the charge distribution on the surface reaches −1.63, indicating the strongest ability to capture hot electrons. Therefore, it can be inferred that the negative charges will

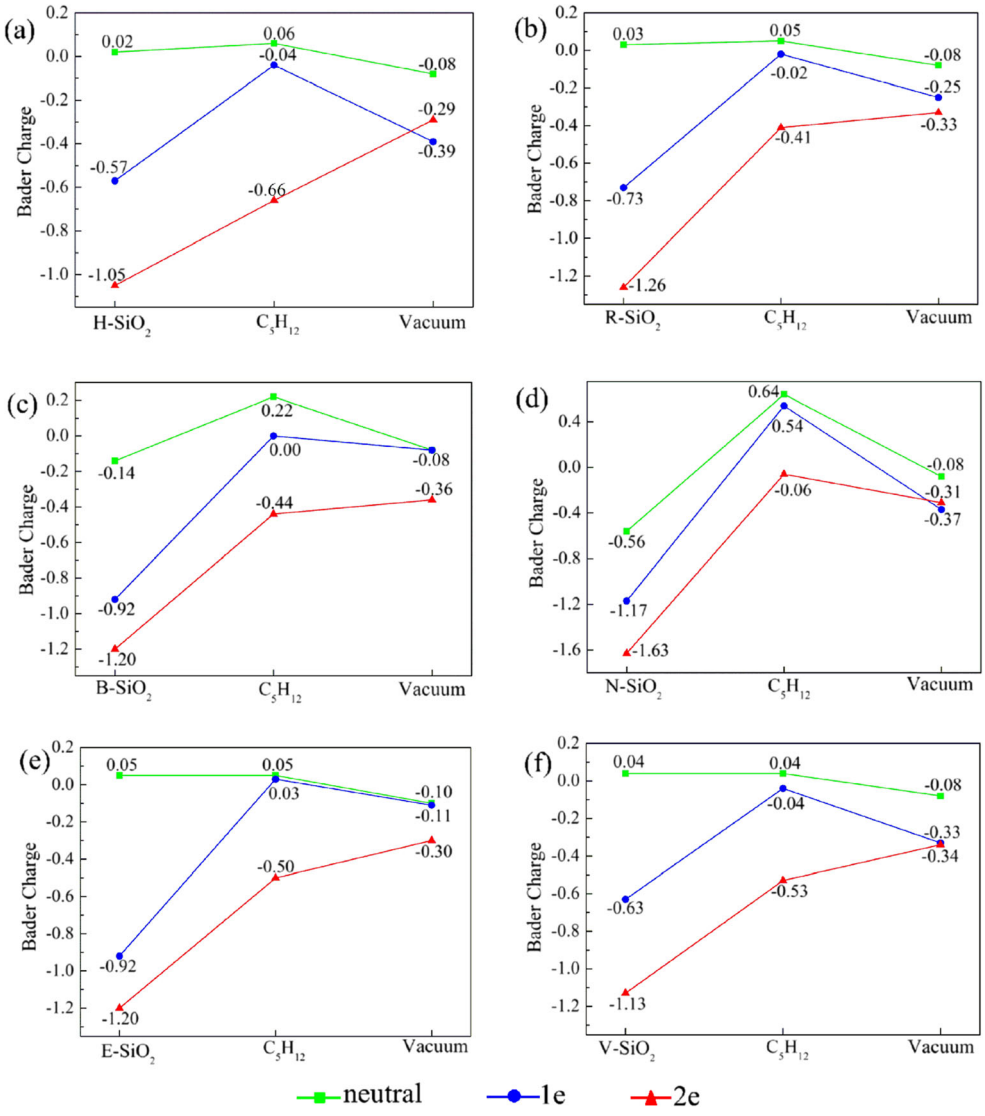

Fig. 4 **a**~**f** The Bader charge distributions of neutral state (in green) and ionic states with one electron injection (in blue) and two electrons injection (in red) for different SiO_2 models

mainly accumulated on SiO_2 additives instead of XLPE. In this way, the XLPE was protected to weaken or avoid the attack of hot electrons. Additionally, we can see from Fig. 4 that part of the negative charges gather in the vacuum layer from −0.11 to −0.39 when excess electrons exist in the system. It means the charge could also be trapped in the middle of the matrix rather than the XLPE chain. As suggested in the experimental measurement for space charge distribution of TiO_2/XLPE nanocomposites, the trapped negative charge in the interface region could shorten the effective distance of "solitary waves" migration, reduce the carrier mobility, weaken the impurity ionization, and finally make the heterocharge disappear [27].

In this way, the interfacial interaction helps the charge transferring out of the XLPE materials.

It is worth noting that all six SiO_2 patterns we studied have the strong capability to capture hot electrons. It means the effect of doping or defect SiO_2 nanoparticles on the space charge distribution is trivial. Similarly, we predict that other various oxygen vacancies of SiO_2, such as nonbridging oxygen hole center (NBOHC), oxygen-deficiency related center (ODC), and silanone groups (SGs) [45], as well as another oxides, such as MgO, Al_2O_3, and TiO_2 etc., will likely have similar properties to trap hot electrons to suppress the growth of electrical tree. It essentially relates to the energy band structures of metal-oxide semi-conductors. Taking SiO_2 as an example, it was well studied in literature that the bottom of the conductive bands is mainly contributed from the 3s and 3p orbitals of the Si atom [49]. Similarly, we calculated the charge density of valence band (VB) and conduction band (CB) for the adsorption models of C_5H_{12} with different SiO_2 surfaces. As shown in Fig. 5, one can see that the VB orbital is around the C_5H_{12} molecule, while the CB orbital mainly locates at the H-SiO_2 or R-SiO_2 substrates. This means that the hot electrons will take precedence to enter into the CB orbital and be trapped by the SiO_2 additives. In the cases of B-SiO_2, N-SiO_2, E-SiO_2, and V-SiO_2, as shown in Suppl. Fig. S1, a similar conclusion could be reached since the dopant or vacancy produces more active sites in the additives to facilitate the attraction for extra electrons. Therefore, the orbital analysis could help us further understand why the additives could effectively trap hot electrons to suppress the electrical tree growth.

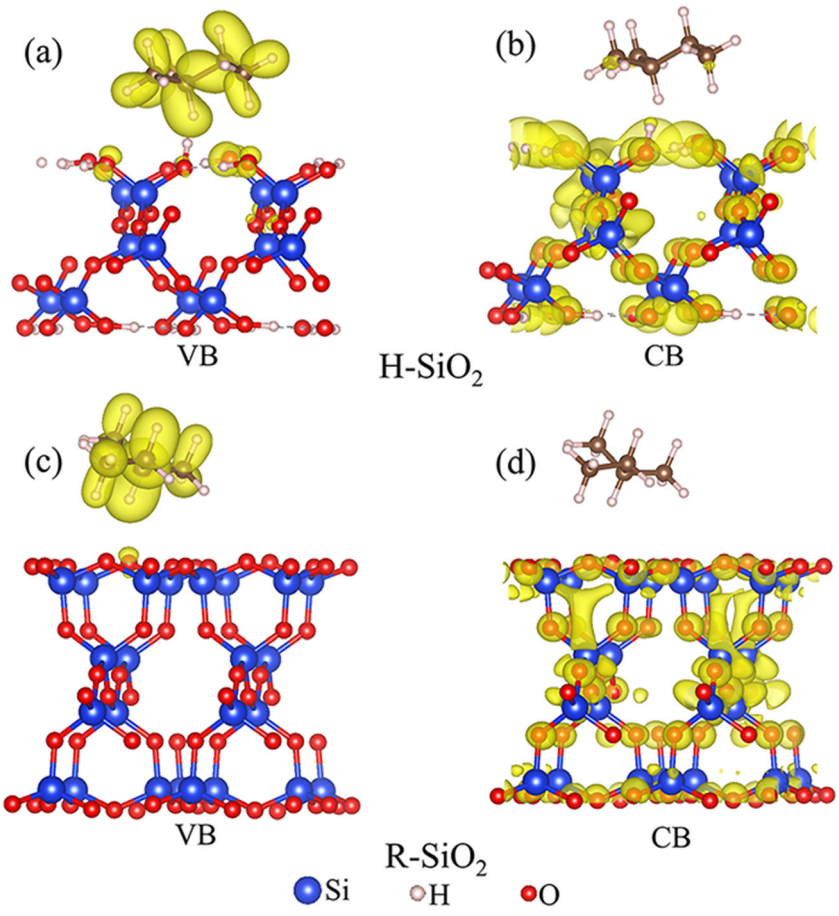

Fig. 5 **a**~**d** The charge density of valence band (VB) and conduction band (CB) for the adsorption models of C_5H_{12} with H-SiO_2 and R-SiO_2

Conclusions

The SiO_2 additives can effectively suppress the space charge accumulation and inhibit electrical tree growth of power cable insulation by constraining the movement of cross-linked polyethylene and trapping hot electrons. We performed density functional theory calculations to screen a series of SiO_2 additives through studying the surface structures, interfacial interaction, H migration reaction activity, and space charge behavior. The SiO_2 with incompletely hydroxylated or boron-doped surfaces are not good candidates as potential additives because they could facilitate the H migration reaction and destroy the XLPE chain. The N-doped SiO_2 with a completely hydroxylated surface is predicted to be the most promising additive among the patterns we studied due to the results of its strongest abilities of adsorption to XLPE and transferring charge, as well as the weakest chemical activity. This information is useful for the experimental treatment of SiO_2 additives and the design of other potential surface-modified SiO_2 additives.

Acknowledgments This work was supported by the National Natural Science Foundation of China (Grant No. 21203041), Natural Science Foundation of Heilongjiang province in China (Grant No. B2016004), the Fundamental Research Funds for the Central Universities in China (Grant No. HIT. NSRIF. 2017033), and the open project of Key Laboratory of Engineering Dielectrics and Its Application (Harbin University of Science and Technology), Ministry of Education, (Grand No. KF20151105).

Compliance with ethical standards

Conflicts of interest There are no conflicts of interest to declare.

References

1. Munteanu D (1997) Moisture cross-linkable silane-modified polyolefins. In: Al-Malaika S (ed) Reactive modifiers for polymers. Springer, Dordrecht, pp 196–265
2. Ramachandran S, Hartlein R, Chandak P (1999) A comparative economic analysis for underground distribution cables insulated with TR-XLPE and EPR. In: IEEE/PES transmission and distribution conference, 11–16 Apr 1999, pp 112–119
3. Pollet P, Liotta CL, Eckert CA, Verma M, Nixon E, Sivaswamy S, Jha R, Momin F, Gelbaum L, Chaudhary BI (2011) Radical-mediated graft modification of polyethylene models with Vinyltrimethoxysilane: a fundamental study. Ind Eng Chem Res 50:12246–12253
4. Mizutani T, Hikita M, Umemura A, Ieda M (1989) Electrical breakdown and space charge of polyphenylene sulfide films. In: Conference on electrical insulation and dielectric phenomena, 29 Oct −01 Nov 1989, pp 315–320
5. Jarvid M, Johansson A, Englund V, Gubanski S (2012) Electrical tree inhibition by voltage stabilizers. In: IEEE conference on electrical insulation and dielectric phenomena, 14–17 Oct 2012, pp 605–608
6. Yin Y, Tu D, Du Q, Gong Z (2000) Distribution and effect of space charge on dielectric properties in modified XLPE by chlorinated polyethylene. In: 6th international conference on properties and applications of dielectric materials, 21–26 Jun 2000, pp 268–271
7. Bradwell A, Cooper R, Varlow B (1971) Conduction in polythene with strong electric fields and the effect of prestressing on the electric strength. Proc IEE 118(1):247–254
8. Du BX, Su JG, Han T (2015) Effects of magnetic field on electrical tree growth in silicone rubber under repetitive pulse voltage. IEEE Trans Dielectr Electr Insul 22(4):1785–1792
9. Werelius P, Tharning P, Eriksson R, Holmgren B (2001) Dielectric spectroscopy for diagnosis of water tree deterioration in XLPE cables. IEEE Trans Dielectr Electr Insul 8(1):27–42
10. Crine JP (1998) Electrical, chemical and mechanical processes in water treeing. IEEE Trans Dielectr Electr Insul 5(5):681–694
11. Englund V, Huuva R, Gubanski SM, Hjertberg T (2009) Synthesis and efficiency of voltage stabilizers for XLPE cable insulation. IEEE Trans Dielectr Electr Insul 16(5):1455–1461
12. Kisin S, Doelder JD, Eaton RF, Caronia PJ (2009) Quantum mechanical criteria for choosing appropriate voltage stabilization additives for polyethylene. Polym Degrad Stab 94(2):171–175
13. Suh KS, Sun Jun H, Lee CR (1997) Charge behavior in polyethylene-ionomer blends. IEEE Trans Dielectr Electr Insul 4(1):58–63
14. Yin Y, Du Q, Gong Z (2000) Influence of blending chlorinated polyethylene on the space charge effect in polyethylene. Trans China Electrotech Soc 15(2):52–57
15. Pleşa I, Noţingher PV, Schlögl S, Sumereder C, Muhr M (2016) Properties of polymer composites used in high-voltage applications. Polymers 8(5):173–176
16. Ieda M, Nagao M, Hikita M (1994) High-field conduction and breakdown in insulating polymers. Present situation and future prospects. IEEE Trans Dielectr Electr Insul 1(5):934–945
17. Vaughan AS, Hosier IL, Dodd SJ, Sutton SJ (2006) On the structure and chemistry of electrical trees in polyethylene. J Phys D Appl Phys 39(5):962–978
18. Chen X, Xu Y, Cao X, Dodd SJ, Dissado LA (2011) Effect of tree channel conductivity on electrical tree shape and breakdown in XLPE cable insulation samples. IEEE Trans Dielectr Electr Insul 18(3):847–860
19. Kurnianto R, Murakami Y, Hozumi N, Nagao M (2007) Characterization of tree growth in filled epoxy resin: the effect of filler and moisture contents. IEEE Trans Dielectr Electr Insul 14(2): 427–435
20. Iizuka T, Tanaka T (2009) Effects of nano silica filler size on treeing breakdown lifetime of epoxy nanocomposites. In: 9th international conference on properties and applications of dielectric materials, 19–23 Jun 2009, pp 733–736
21. Tanaka T, Iizuka T, Sekiguchi Y, Murata Y (2009) Tree initiation and growth in LDPE/MgO nanocomposites and roles of nano fillers. In: Annual report conference on electrical insulation and dielectric phenomena, 18–21 Oct 2009, pp 646–649
22. Tanaka T, Bulinski A, Castellon J, Frechette M, Gubanski S, Kindersberger J, Montanari GC, Nagao M, Morshuis P, Tanaka Y, Pelissou S, Vaughan A, Ohki Y, Reed CW, Sutton S, Han SJ (2011) Dielectric properties of XLPE/SiO_2 nanocomposites based on CIGRE WG D1.24 cooperative test results. IEEE Trans Dielectr Electr Insul 18(5):1482–1517
23. Zhang L, Zhou Y, Huang M, Sha Y, Tian J, Ye Q (2014) Effect of nanoparticle surface modification on charge transport characteristics in XLPE/SiO_2 nanocomposites. IEEE Trans Dielectr Electr Insul 21(2):424–433
24. Li Z, Okamoto K, Ohki Y, Tanaka T (2011) The role of nano and micro particles on partial discharge and breakdown strength in epoxy composites. IEEE Trans Dielectr Electr Insul 18(3):675–681
25. Ding HZ, Varlow BR (2004) Effect of nano-fillers on electrical treeing in epoxy resin subjected to AC voltage. In: Annual

conference on electrical insulation and dielectric phenomena (CEIDP), 17–20 Oct 2004, pp 332–335
26. Wang Y, Wang C, Xiao K (2016) Investigation of the electrical properties of XLPE/SiC nanocomposites. Polym. Test. 50:145–151
27. Wang Y, Xiao K, Wang C, Yang L, Wang F (2016) Study on dielectric properties of TiO_2/XLPE nanocomposites. In: IEEE international conference on high voltage engineering and application (ICHVE), 19–22 Sept 2016, pp 1–4
28. Han B, Jiao M, Li C, Zhang C, Wu Z, Wang Y, Zhang H (2015) QM/MD simulations on the role of SiO_2 in polymeric insulation materials. RSC Adv 6(1):555–562
29. Song S, Zhao H, Zheng X, Zhang H, Liu Y, Wang Y, Han B (2018) A density functional theory study of the role of functionalized graphene particles as effective additives in power cable insulation. R Soc Open Sci 5(2):170772
30. Hickel PE, Lafon F, Fortis F, Cambon O, Demazeau G (1997) On the development of new solvents for the high pressure crystal growth of α-quartz. Ann Chim-Sci Mat 22(8):571–576
31. Hickel PE, Lafon F, Chvansky PP, Largeteau A, Demazeau G (1997) Influence of the different physico-chemical parameters governing the crystal growth of α-quartz on the concentration of chemical defects. Ann Chim-Sci Mater 22(8):583–588
32. Balascio JF, Lind T (1997) The growth of piezoelectric alpha quartz crystals. Curr Opin Solid State Mater Sci 2(5):588–592
33. de Leeuw NH, Higgins FM, Parker SC (1999) Modeling the surface structure and stability of α-quartz. J Phys Chem B 103(8):1270–1277
34. Wegener J, Janshoff A, Steinem C (2001) The quartz crystal microbalance as a novel means to study cell-substrate interactions in situ. Cell Biochem Biophys 34(1):121–151
35. Du B, Johannsmann D (2004) Operation of the quartz crystal microbalance in liquids: derivation of the elastic compliance of a film from the ratio of bandwidth shift and frequency shift. Langmuir 20(7):2809–2812
36. Ayad MM, Zaki EA, Stejskal J (2007) Determination of the dopant weight fraction in polyaniline films using a quartz-crystal microbalance. Thin Solid Films 515(23):8381–8385
37. Goumans TPM, Wander A, Brown WA, Catlow CRA (2007) Structure and stability of the (001) alpha-quartz surface. Phys Chem Chem Phys 9(17):2146–2152
38. Han JW, James JN, Sholl DS (2008) First principles calculations of methylamine and methanol adsorption on hydroxylated quartz (0001). Surf Sci 602(14):2478–2485
39. Rignanese GM, De Vita A, Charlier JC, Gonze X, Car R (2000) First-principles molecular-dynamics study of the (0001) α−quartz surface. Phys Rev B 61(19):13250–13255
40. Chen Y-W, Cao C, Cheng H-P (2008) Finding stable α-quartz (0001) surface s tructures via simulations. Appl Phys Lett 93(18): 181911
41. Jánossy I, Menyhárd M (1971) LEED study of quartz crystals. Surf Sci 25(3):647–649
42. Bart F, Gautier M (1994) A LEED study of the (0001) a-quartz surface reconstruction. Surf. Sci. 311(1–2):L671–L676
43. Koudriachova MV, Beckers JVL, de Leeuw SW (2001) Computer simulation of the quartz surface: a combined ab initio and empirical potential approach. Comput Mater Sci 20(3):381–386
44. Del Rosal I, Gerber IC, Poteau R, Maron L (2015) Grafting of lanthanide complexes on silica surfaces dehydroxylated at 200 °C: a theoretical investigation. New J Chem 39(10):7703–7715
45. Skuja L, Kajihara K, Hirano M, Hosono H (2012) Oxygen-excess-related point defects in glassy/amorphous SiO_2 and related materials. Nucl Instrum Methods Phys Res B 286:159–168
46. Nicklaw CJ, Pagey MP, Pantelides ST, Fleetwood DM, Schrimpf RD, Galloway KF, Wittig JE, Howard BM, Taw E, McNeil WH, Conley JF (2000) Defects and nanocrystals generated by Si implantation into a-SiO_2. IEEE Trans Nucl Sci 47(6):2269–2275
47. Chandrasekhar PS, Komarala VK (2015) Effect of graphene and au@SiO_2 core-shell nano-composite on photoelectrochemical performance of dye-sensitized solar cells based on N-doped titania nanotubes. RSC Adv 5(103):84423–84431
48. Zhao X, He XD, Zhang S, Wang LD, Li MW, Li YB (2011) Investigations on B-doped SiO_2 thermal protective coatings by hybrid sol–gel method. Thin Solid Films 519(15):4849–4854
49. Zhang SS, Zhao ZY, Yang PZ (2015) Analysis of electronic structure and optical properties of N-doped SiO_2 based on DFT calculations. Mod Phys Lett B 29(19):1550100
50. Pacchioni G, Vezzoli M, Fanciulli M (2001) Electronic structure of the paramagnetic boron oxygen hole center in B-doped SiO_2. Phys Rev B 64(15):155201
51. Kresse G, Furthmüller J (1996) Efficient iterative schemes for ab initio total-energy calculations using a plane-wave basis set. Phys Rev B 54(16):11169–11186
52. Kresse G, Hafner J (1993) Ab initio molecular dynamics for liquid metals. Phys Rev B 47(1):558–561
53. Kresse G, Hafner J (1994) Norm-conserving and ultrasoft pseudopotentials for first-row and transition elements. J Phys Condens Matter 6(40):8245–8257
54. Perdew JP, Burke K, Ernzerhof M (1996) Generalized gradient approximation made simple. Phys Rev Lett 77(18):3865–3868
55. Blöchl PE, Jepsen O, Andersen OK (1994) Improved tetrahedron method for Brillouin-zone integrations. Phys Rev B 49(23):16223–16233
56. Bader RFW (1991) A quantum theory of molecular structure and its applications. Chem Rev 91(5):893–928
57. Bader RFW (1994) Atoms in molecules: a quantum theory. THEOCHEM J Mol Struct 360(1–3):175
58. Pan D, Liu L-M, Tribello GA, Slater B, Michaelides A, Wang E (2008) Surface energy and surface proton order of ice Ih. Phys Rev Lett 101(15):155703
59. Henkelman G (2000) Improved tangent estimate in the nudged elastic band method for finding minimum energy paths and saddle points. J Chem Phys 113(113):9978–9985
60. Henkelman G, Uberuaga BP, Jónsson H (2000) A climbing image nudged elastic band method for finding saddle points and minimum energy paths. J Chem Phys 113(22):9901–9904
61. Liu Q, Poumellec B, Blum R, Girard G (2006) Stability of electron-beam poling in N or Ge-doped H:SiO_2 films. Appl Phys Lett 88(24):693
62. Weidner DJ (1980) Structure and elastic properties of quartz at pressure. Am Mineral 65(2):920–930
63. Malyi OI, Kulish VV, Persson C (2014) In search of new reconstructions of (001) α-quartz surface: a first principles study. RSC Adv 4(98):55599–55603
64. Pacchioni G (2000) Ab initio theory of point defects in oxide materials: structure, properties, chemical reactivity. Solid State Sci 2(2):161–179
65. Raghavachari K, Ricci D, Pacchioni G (2002) Optical properties of point defects in SiO_2 from time-dependent density functional theory. J Chem Phys 116(2):825–831